

■ Electrochemistry | *Hot Paper* |

Catechol-Coordinated Framework Film-based Micro-Supercapacitors with AC Line Filtering Performance

Tianliang Yu,^[a, b] Youfu Wang,^[b] Kaiyue Jiang,^[b, e] Guangqun Zhai,^{*,[a]} Changchun Ke,^{*,[c]} Jichao Zhang,^[f] Jiantong Li,^[d] Diana Tranca,^[b] Emmanuel Kymakis,^[g] and Xiaodong Zhuang^{*,[b]}

Abstract: Coordination polymer frameworks (CPFs) have broad applications due to their excellent features, including stable structure, intrinsic porosity, and others. However, preparation of thin-film CPFs for energy storage and conversion remains a challenge because of poor compatibility between conductive substrates and CPFs and crucial conditions for thin-film preparation. In this work, a CPF film was prepared by the coordination of the anisotropic four-armed ligand and Cu^{II} at the liquid–liquid interface. Such film-based micro-supercapacitors (MSCs) are fabricated through high-energy scribing and electrolytes soaking. As-fabricated MSCs

displayed high volumetric specific capacitance of 121.45 F cm⁻³. Besides, the volumetric energy density of MSCs reached 52.6 mWh cm⁻³, which exceeds the electrochemical performance of most reported CPF-based MSCs. Especially, the device exhibited alternating current (AC) line filtering performance (−84.2° at 120 Hz) and a short resistance capacitance (RC) constant of 0.08 ms. This work not only provides a new CPF for MSCs with AC line filtering performance but also paves the way for thin-film CPFs preparation with versatile applications.

Introduction

With the rapid development of portable and wearable electronic devices, lightweight, miniaturized, and efficient energy storage devices become more and more important.^[1] Commercially available micro-batteries have already shown great potential in this field. However, batteries still have intrinsic problems of low power density and limited cycling performance, hindering their application as reliable micro-power sources.^[2] As a novel energy storage device, electrochemical capacitors

(or supercapacitors)^[3] possess obvious superiority, such as high power density, long cycle lifetime, fast charge and discharge rates, and compatibility of integration with various electronic components.^[4] Recent studies have found that thin-film-based flat micro-supercapacitors (MSCs)^[5] based on nanostructured functional materials, such as graphene,^[6] graphene-based nanocomposites,^[7] monolithic carbide-derived carbon,^[4a] polymer films,^[8] and others, can provide new components for modern on-chip integrated circuits. However, most of the devices based on these materials demand multiple processing

[a] T. Yu, Prof. G. Zhai
meso-Entropy Matter Lab
Jiangsu Key Laboratory of Environmentally Friendly Polymeric Materials
School of Materials Science and Engineering
Changzhou University
Changzhou 213164 (China)
E-mail: zhai_gq@cczu.edu.cn

[b] T. Yu, Y. Wang, K. Jiang, Dr. D. Tranca, Prof. X. Zhuang
Themeso-Entropy Matter Lab
State Key Laboratory of Metal Matrix Composites
Shanghai Key Laboratory of Electrical Insulation and Thermal Ageing
School of Chemistry and Chemical Engineering
Frontiers Science Center for Transformative Molecules
Shanghai Jiao Tong University
800 Dongchuan Road, Shanghai 200240 (China)
E-mail: zhuang@sytu.edu.cn

[c] Dr. C. Ke
Institute of Fuel Cells
School of Mechanical Engineering
Shanghai Jiao Tong University
Shanghai 200240 (China)
E-mail: kechangchun@sytu.edu.cn

[d] Dr. J. Li
School of Electrical Engineering and Computer Science
KTH Royal Institute of Technology
Electrum 229, 16440 Kista (Sweden)

[e] K. Jiang
College of Chemistry and Molecular Engineering
Zhengzhou University
Zhengzhou 450001, Henan (China)

[f] Dr. J. Zhang
Shanghai Synchrotron Radiation Facility
Zhangjiang Laboratory
Shanghai Advanced Research Institute
Chinese Academy of Sciences, No. 239
Zhangheng Road, Shanghai 201204 (China)

[g] Prof. E. Kymakis
Department of Electrical & Computer Engineering
Hellenic Mediterranean University
Estavromenos, 71410 Heraklion (Greece)

 Supporting information and the ORCID identification number(s) for the author(s) of this article can be found under:
 <https://doi.org/10.1002/chem.202100171>.

steps, such as complicated photolithography processes or high-temperature preparation of electrode materials. The development of MSCs through a simple fabrication process is significant for their practical applications.

Alternating current (AC) line filtering is one of the most important features of MSCs and can be used to filter AC ripple on the line-powered devices.^[9] As one of the paramount properties of renewable electronic power systems, AC line filtering can be used for power generation. However, only commercially available aluminum electrolytic capacitors (AECs) can be used for such application and suffer from low energy density and bulky volume dimensions. Therefore, AECs are not compatible with fast-developing portable electronic devices. So far, porous carbon-based supercapacitors have shown promising AC line filtering performance. However, the slow response of the polarization, limited signal propagation, and poor film formation property of porous carbons hinder the practical application. Development of new materials with AC line filtering performance remains a great challenge.

Herein, a coordination polymer framework (CPF) film is synthesized by a liquid–liquid interfacial method based on an anisotropic four-armed ligand. Such framework film based on catechol-Cu node shows uniform thickness, a large horizontal area reaching several square centimeters, and a narrow band gap of 0.84 eV. As electrode material for MSCs, such film can achieve areal and volumetric specific capacitances of 2.89 mFcm⁻² and 121.45 Fcm⁻³, respectively. Moreover, the MSC exhibits a high energy density of 52.6 mWhcm⁻³ and power density of 13.1 Wcm⁻³. Noteworthy, the device shows promising AC line filtering performance (−84.2° at 120 Hz) and a short resistance capacitance (RC) time constant (τ_{RC}) of 0.08 ms. This work provides a new material option for the fabrication of MSCs with AC line filtering performance.

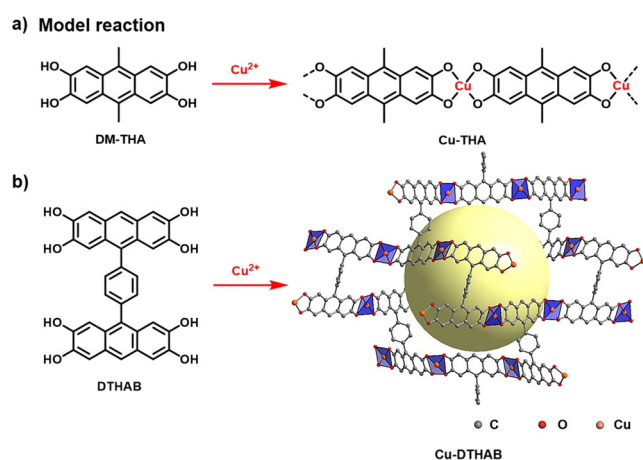
Results and Discussion

The preparation of CPF and control linear coordination polymer Cu-THA is illustrated in Scheme 1. CPF was prepared by the coordination of the ligand 9,9'-(1,4-phenylene)bis(anthra-

cene-2,3,6,7-tetraol) (denoted as DTHAB, Scheme S1) and Cu²⁺ in solution. Both of the monomers, DTHAB and DM-THA (9,10-dimethyl-2,3,6,7-tetrahydroxyanthracene, Scheme S2), possess anisotropic topology. The synthesis and characterizations can be found in the Experimental Section and Supporting Information (Figures S1–S16).

X-ray absorption fine structure (XAFS) and extended X-ray absorption fine structure (EXAFS) techniques were employed to analyze the electronic structure and coordination geometry of Cu-DTHAB in comparison with Cu foil, CuO, and Cu₂O. As shown in Figure 1 a, the enlarged pre-edge of Cu-DTHAB locates between CuO and Cu₂O, indicating that the average valence state of Cu atoms is between +2 and +1.^[10] Meanwhile, the Fourier-transform (FT) EXAFS oscillation spectrum of Cu-DTHAB (Figure 1 b) presents a predominant peak at 1.57 Å, which originates from the Cu–O bond,^[11] suggesting the coordination of Cu ions with DTHAB. Moreover, least-squares EXAFS fitting is carried out to realize quantitative structural parameters of Cu in Cu-DTHAB (Figure S17a), indicating the coordination number of Cu is 4 (Table S1). Wavelet transform (WT) (WT-EXAFS) is also performed to analyze the atomic dispersion of Cu atoms (Figure S17b). The intensity maximum at 6.5 Å⁻¹ is attributed to the Cu–O contribution for Cu-DTHAB.^[12] To further study the chemical structure of the Cu-DTHAB, X-ray photoelectron spectroscopy (XPS) was employed. The survey XPS spectrum (Figure S18) is dominated by C, O, Cu peaks. The O 1s core level spectrum (Figure 1 c) reveals the O–Cu peak at 532.4 eV, and the residual O peak at 533.7 eV, demonstrating the coordination between O and Cu atoms.^[13] In addition, Cu 2p core level spectrum (Figure 1 d) consists of the Cu^{II}2p_{3/2} peak at 935.1 eV, Cu^I2p_{3/2} peak at 935.1 eV, Cu^{II}2p_{1/2} peak at 952.6 eV, Cu^I2p_{1/2} peak at 954.2 eV, as well as the shake-up satellite peaks at 959.8–967.1 and 938.7–948.6 eV.^[14] The XPS spectrum of Cu-THA was also analyzed and shows similar phenomena (Figure S19). To further verify the coordination of catechol units and copper ions, the chemical structures of DTHAB and Cu-DTHAB were studied through Fourier-transform infrared (FTIR) spectroscopy (Figure S20a) and Raman spectroscopy. Compared to the FTIR spectrum of DTHAB, the reduced O–H stretching band at approximately 3228 cm⁻¹ indicates the prosperous coordination between the phenolic hydroxy and copper ions. Moreover, the band centered at 1266 cm⁻¹ for Cu-DTHAB exhibits a distinct transformation to higher energy compared with the C–O stretching at 1234 cm⁻¹ for DTHAB.^[13] Meanwhile, the phenolic hydroxyl peak at approximately 3169 cm⁻¹ of the Cu-DTHAB (Figure S21a) disappeared by comparing with DTHAB. All these results indicate that the proposed structure was successfully realized through coordination between Cu^{II} and catechol.

Furthermore, the optoelectronic properties of Cu-DTHAB were studied. The ultraviolet-visible absorption spectrum was tested by UV/Vis-NIR spectroscopy (Figure S22). The optical band gap could be calculated from the UV/Vis absorption edge (Figure 2 a). Cu-DTHAB reveals a band gap of 0.84 eV according to the Kubelka–Munk (K–M) function.^[15] The UV photoelectron spectroscopy (UPS, Figure 2 b) was further used to determine the valence band (E_{VB}). The E_{VB} of −4.83 eV (vs.



Scheme 1. Synthesis of Cu-THA and Cu-DTHAB.

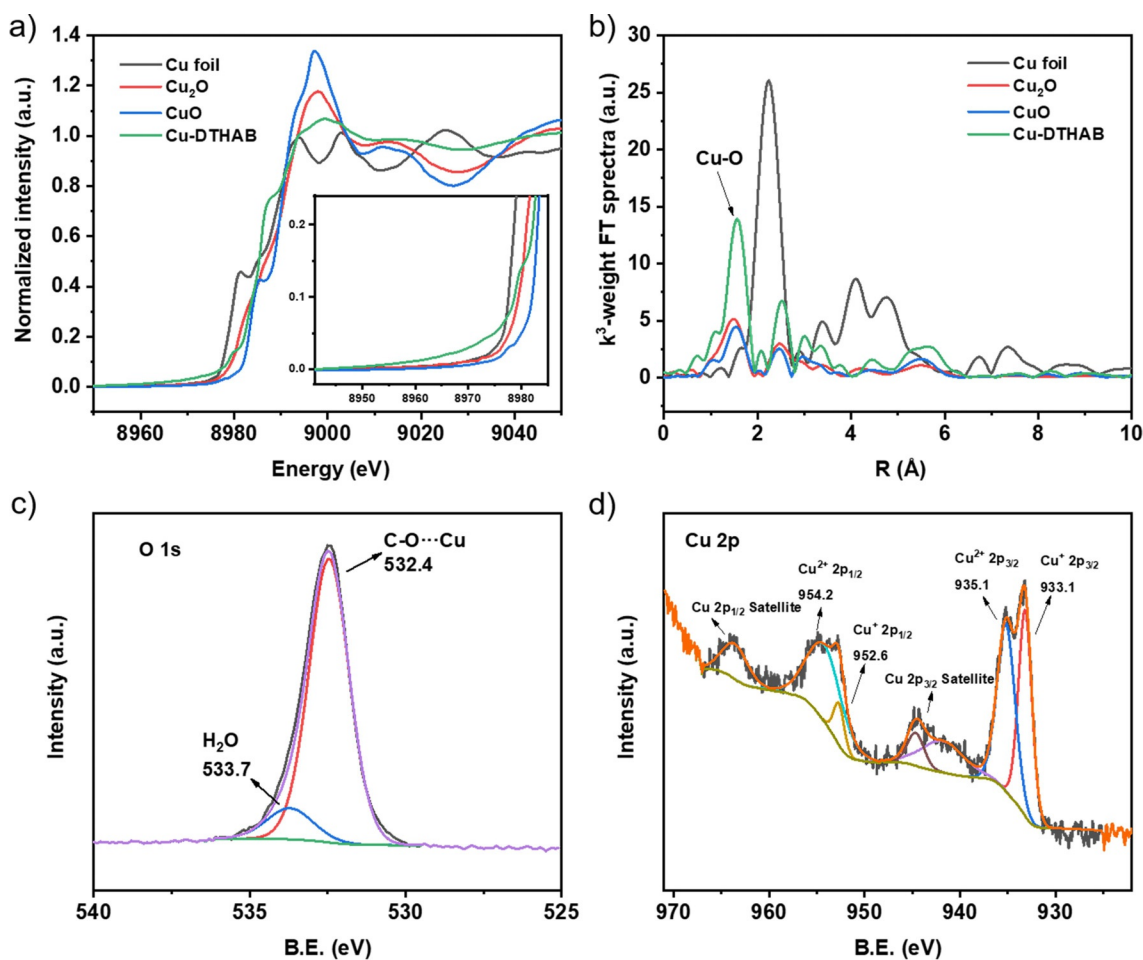


Figure 1. (a) Normalized XANES spectra of Cu-DTHAB, Cu foil, CuO, and Cu₂O. (b) Fourier transformation EXAFS spectra of Cu-DTHAB with Cu foil, CuO, and Cu₂O as control samples. (c) O 1s XPS spectrum of Cu-DTHAB. (d) Cu 2p XPS spectrum of Cu-DTHAB.

vacuum level) was calculated according to a well-established method.^[16] Then, the conduction band (E_{CB}) can be calculated as -3.99 eV (vs. vacuum level) based on optical band gap (Figure 2c). The cyclic voltammetry (CV) curves of Cu-DTHAB and DTHAB were investigated in CH₃CN at 20 mV s⁻¹ (Figure 2d). The highest occupied molecular orbital (HOMO) and lowest unoccupied molecular orbital (LUMO) levels of Cu-DTHAB are significantly different from those of DTHAB. The calculated band gap according to CV curves ($E_{g,CV}$) of Cu-DTHAB (1.14 eV) is smaller than that of DTHAB (1.67 eV). Meanwhile, the CV curves of Cu-THA and DM-TMA (Figure S23) were also employed through the same test method, the $E_{g,CV}$ of Cu-THA (1.22 eV) is also smaller than DM-TMA (1.55 eV). These results demonstrate the semiconducting properties of the Cu-DTHAB and Cu-THA.

To better estimate the electronic structures of the Cu-DTHAB framework, density functional theory (DFT) was used for calculation. Figure 3a,b shows the possible three-dimensional (3D) and two-dimensional (2D) models of the Cu-DTHAB (denoted as Cu-DTHAB-3D and Cu-DTHAB-2D, respectively). Figure 3c shows the model of the control sample Cu-THA. The calculated density of states (DOS) curves (Figure 3d) reveal narrower band gaps of Cu-DTHAB-3D, Cu-DTHAB-2D, and Cu-THA of

0.92 , 0.68 , and 0.58 eV, respectively. As is known, 3D structure should be the preferred structure for Cu-DTHAB because of the free rotated C–C bonds between benzene and anthracene of DTHAB. The calculated band gap of Cu-DTHAB-3D (0.92 eV) is close to the optical band gap (0.84 eV) and CV-based band gap (1.14 eV), indicating the preferred 3D structure for Cu-DTHAB.

The porosity of Cu-DTHAB was studied by nitrogen physical adsorption measurement (Figure S24). The Brunauer–Emmett–Teller (BET) surface area of Cu-DTHAB is 127 m²g⁻¹. The pore volume and pore diameter of Cu-DTHAB are 0.29 cm³g⁻¹ and 8.7 nm (Table S2), respectively. The thermogravimetric analysis (TGA) curve of Cu-DTHAB (Figure S25a) shows mass loss by 6.6% at 200 °C, indicating good thermal stability of the structure. The TGA curve of DTHAB was also recorded for better comparison to Cu-DTHAB (Figure S25b). To investigate the magnetic character of the Cu-DTHAB, magnetization measurements were performed through a superconducting quantum interference device-vibrating sample magnetometer (SQUID-VSM, Figure S26). It embodies the variation of the magnetization with the applied magnetic field (H) measured at 298 K, a sigmoidal shape of $M(H)$ signs the weak ferromagnetism behavior.^[17] In addition, the solid-state electron paramagnetic res-

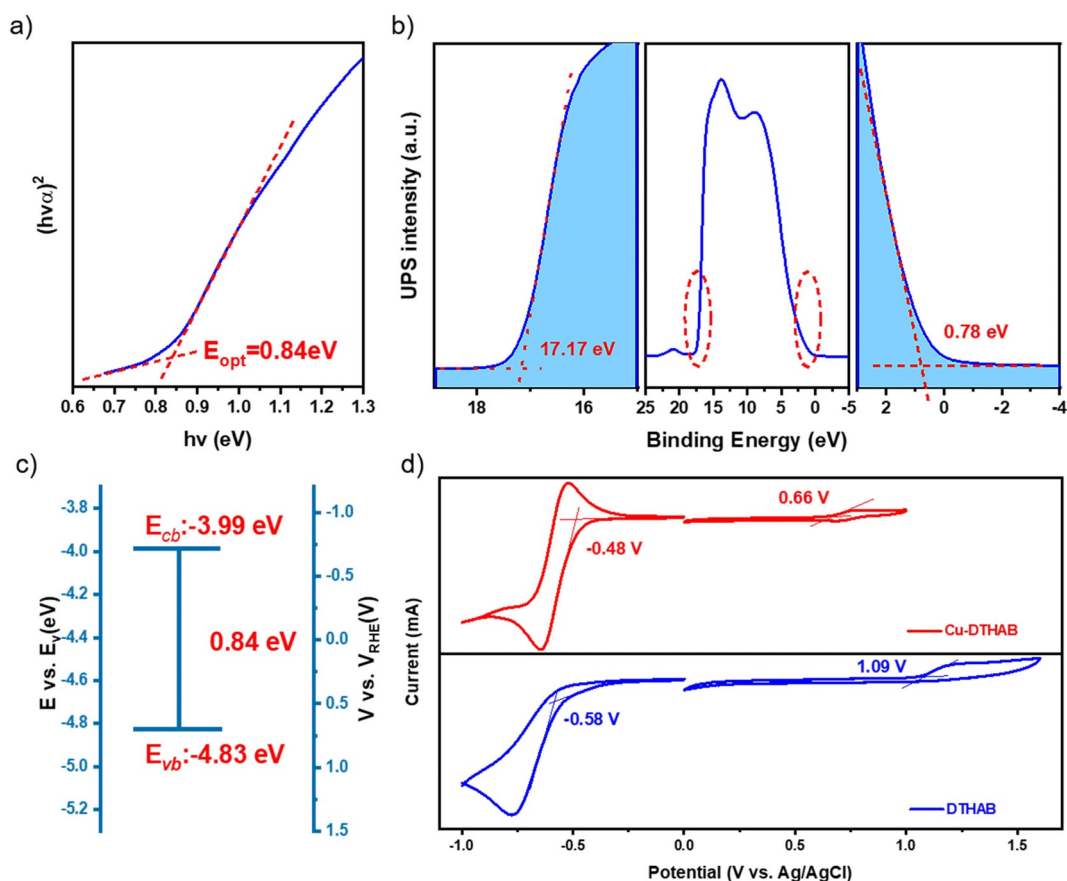


Figure 2. (a) $(h\nu c_{\alpha})^2$ against $h\nu$ curve of Cu-DTHAB. (b) UPS spectrum of Cu-DTHAB. (c) E_{cb^*} and E_{vb^*} positions of Cu-DTHAB. (d) CV profiles of Cu-DTHAB and DTHAB measured in CH_3CN at a scan rate of 20 mVs^{-1} . $E_{\text{HOMO}} = -(E_{\text{ox}} + 4.42 \text{ eV})$; $E_{\text{LUMO}} = -(E_{\text{red}} + 4.42 \text{ eV})$; $E_{\text{g,CV}} = E_{\text{HOMO}} - E_{\text{LUMO}}$.

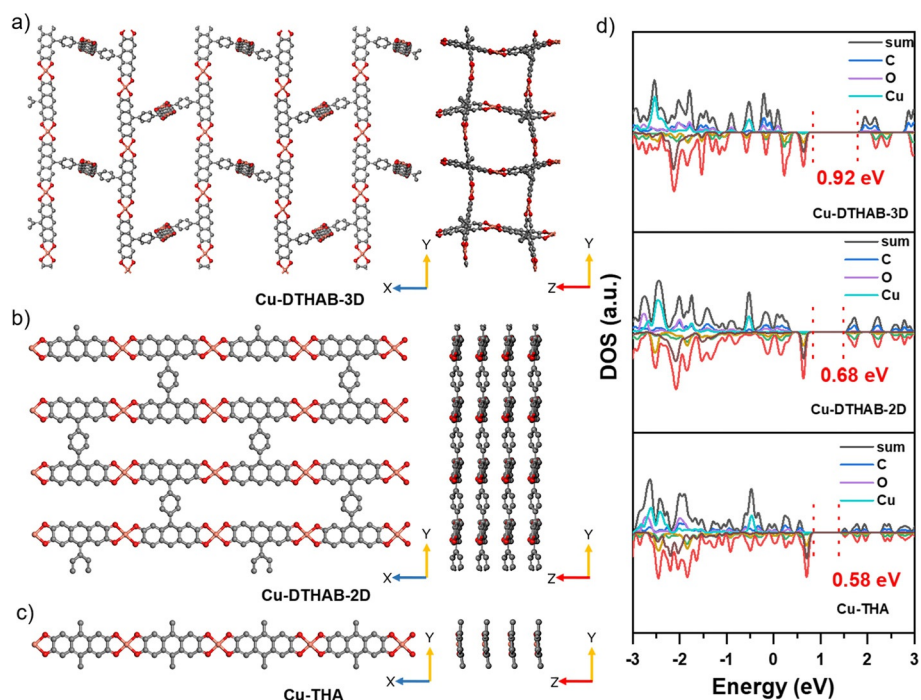


Figure 3. Models of Cu-DTHAB in 3D (a) and 2D (b) configurations and the control linear polymer Cu-THA (c). Grey: C; red: O; orange: Cu. (d) Calculated density of states of Cu-DTHAB-3D, Cu-DTHAB-2D and Cu-THA.

onance (EPR) was also employed to analyze the distribution of unpaired electrons in the Cu-DTHAB (Figure S27). A nearly symmetrical signal is displayed at $g=2.10$, which is the behavior of the metal-centered radicals.^[18]

A series of thin Cu-DTHAB films were performed by liquid-liquid interfacial polymerization for the preparation of micro-supercapacitors. The procedure is shown in Figure 4a. In short, the Cu-DTHAB films (Figure 4b) were transferred to Au substrate. Then Cu-DTHAB/Au films were laser-scribed to prepare interdigitated electrodes.^[8b] After appending electrolyte and solidification overnight, Cu-DTHAB based MSCs (denoted as MSC-Cu-DTHAB) can be obtained. Cu-DTHAB films with an average thickness of 240 ± 5 nm were used to perform flat MSCs (Figure 4c). As-prepared Cu-DTHAB films have continuous and uniform characteristics (SEM, Figure S28). Meanwhile, the elemental mapping images (Figure S29) suggest the C, O and Cu are evenly distributed in Cu-DTHAB. The SEM images (Figure 4d) of the as-fabricated MSC-Cu-DTHAB show glossy edges along the interdigital finger electrodes. In addition, the mechanical properties (elastic modulus and hardness) of Cu-DTHAB film were characterized through Nano Indentor (Table S3), which show such film has a certain mechanical strength.

The electrochemical performance of the MSC-Cu-DTHAB was researched through CV from 10 mV s^{-1} to 1.0 V s^{-1} in different electrolytes (PVA/LiCl, PVA/H₂SO₄ and [EMIM][BF₄]). It can be seen from Figures S30a, S31a, and S32a, MSC-Cu-DTHAB shows an obvious pseudocapacitive effect with redox peaks. The areal and volumetric specific capacitances of MSC-Cu-DTHAB can be calculated through CV curves (Figure 5a). The MSC-Cu-DTHAB exhibits the high volumetric specific capacitance of 121.45 F cm^{-3} in PVA/LiCl electrolyte at a scan rate of 10 mV s^{-1} , which exceeds the value of most reported polymer-

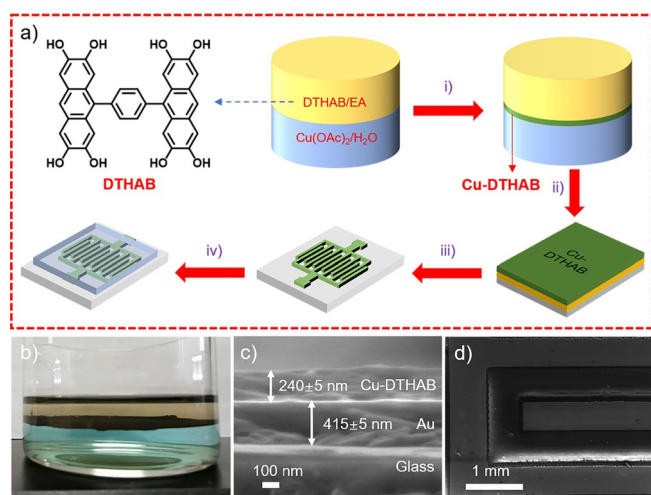


Figure 4. (a) Schematic illustration of fabricating Cu-DTHAB film-based MSC. i) Synthesis of Cu-DTHAB films using liquid-liquid polymerization; ii) transferring Cu-DTHAB films onto Au current collector; iii) laser scraping Cu-DTHAB/Au heterolayer to fabricate an interdigital pattern; iv) drop-casting and solidification gel electrolytes onto interdigitated fingers to fabricate Cu-DTHAB based MSCs. (b) Photograph of the formed Cu-DTHAB film. (c) Profile of Cu-DTHAB film. (d) SEM image of interdigital finger electrodes on a glass.

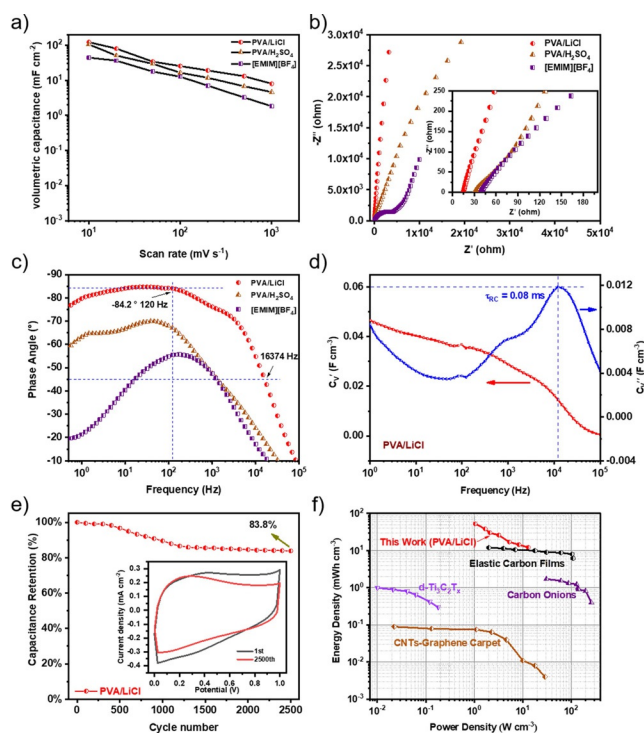


Figure 5. MSCs performance in PVA/LiCl, PVA/H₂SO₄, and [EMIM][BF₄]. (a) Rate-dependent specific volumetric capacitance. (b) Nyquist plots. (c) Impedance phase angles on the frequency. (d) Plot of capacitance (C_v and C_v') versus the frequency of MSC-Cu-DTHAB. (e) Cycling stability of MSC-Cu-DTHAB at the scan rate of 50 mV s^{-1} . (inset: the 1st and 2500th CV curves of MSC-Cu-DTHAB at the scan rate of 50 mV s^{-1}). (f) Ragone plots for MSC-Cu-DTHAB.

based supercapacitors (Table S4). The volumetric specific capacitance maintains 7.98 F cm^{-3} at a high scan rate of 1 V s^{-1} , demonstrating a high capacitance and rate performance of MSC-Cu-DTHAB.

Meanwhile, the electrochemical impedance spectroscopy (EIS) was employed to research the frequency response of MSC-Cu-DTHAB based on different electrolytes (Figure 5b). The minimum values of equivalent series resistance (ESR) were found to be 15.02, 30.2, and 39.53Ω in different electrolytes (PVA/LiCl, PVA/H₂SO₄, and [EMIM][BF₄]), respectively.^[19] The Nyquist plot of the MSC-Cu-DTHAB based on [EMIM][BF₄] contains a small arc in the initial position. The frequency-dependent phase angle (Figure 5c) indicates capacitive and inductive behavior at frequencies.^[9b] The phase angle of the device reaches -84.7° at frequency of approximately 26 Hz, indicating that the performance of the MSCs is 94.1% of an ideal capacitor (defined by a phase angle of -90°).^[20] In addition, the characteristic frequency (f_0) of the system, corresponding to the maximum of the dispersed energy curve (obtained from the phase angle of 45°) is 16374 Hz in PVA/LiCl, 1312 Hz in PVA/H₂SO₄, and 1281 Hz in [EMIM][BF₄]. The f_0 value for MSCs is a specific balance point where the resistive value is equal to the value of capacitive impedance. Therefore, the corresponding time constant τ_0 ($\tau_0 = 1/f_0$) can be calculated as 0.06, 0.76, and 0.78 ms for the MSC-Cu-DTHAB in PVA/LiCl, PVA/H₂SO₄, and [EMIM][BF₄], respectively.^[8a] Moreover, MSC-Cu-DTHAB shows an im-

pedance phase angle of -84.2° at 120 Hz, indicating promising AC line filtering performance (Table S5).^[21] The calculated RC time constant (τ_{RC}) based on the imaginary capacitance (Figure 5d) is 0.08 ms in MSC-Cu-DTHAB. The cycling test was investigated at a routine scan rate of 50 mV s^{-1} over 2500 cycles (Figure 5e). The first circle and the 2500th circle CV shapes are relatively close. The capacitance retention of 83.8% can be achieved after 2500 cycles, indicating good stability for MSC-Cu-DTHAB. MSC-Cu-DTHAB exhibits a high energy density of 52.6 mWh cm^{-3} at 0.05 mA cm^{-2} (Figure 5f); the value is higher than most recently reported functional materials-based supercapacitors, such as CNTs-graphene carpets,^[21] $d\text{-Ti}_3\text{C}_2\text{T}_x$,^[4a] and elastic carbon films and carbon onions.^[22] These results suggest that the prepared Cu-DTHAB film is a promising electrode material for MSCs.

To further understand the energy storage mechanism of Cu-DTHAB, electrochemical quartz crystal microbalance (EQCM) measurement was used to reveal the mass changes and viscoelastic properties of the electrodes during charge-discharging in $1.0 \text{ mol L}^{-1} \text{ H}_2\text{SO}_4$.^[23] Figure S34a shows the frequency, potential and response resistance curves with time. The resonance resistance does not show a particularly large response, and it is stable in a small range ($\pm 7 \Omega$). Therefore, it satisfies the conditions of the Sauerbrey equation. The CV curve and mass changes of Cu-DTHAB at 10 mV s^{-1} were displayed in Figure S34b. During the potential increasing process from 0 to 1 V, the electrode mass increased. When the potential reaches the maximum, the electrode mass also reaches the maximum value, indicating the adsorbed ions reach the maximum. After a cycle, the electrode mass becomes slightly smaller. Figure S34c shows the relationship between experimental and theoretical ion population changes (ΔI) and charge density (ΔQ) during the charging and discharging process. The adsorption of H_3O^+ ions was considered, and exactly M_i of 19 g mol^{-1} for ΔI_{theor} and ΔI_{exp} was a good coincidence. In addition, the capacitance of MSC-Cu-DTHAB has the behavior of double-layer capacitance (C_{dl}) and pseudocapacitance (C_p). The respective capacitance contribution was researched using Trasatti analysis. The plot of reciprocal of areal capacitance (C^{-1}) against the square root of scan rate ($v^{0.5}$) and the plot of areal capacitance (C) against reciprocal of the square root of scan rate ($v^{-0.5}$) was displayed in Figure S35. The total capacitance contributions from C_{dl} and C_p were calculated through the Trasatti method are 74 and 26%, respectively,^[24] which quantitatively analyzes the pseudocapacitance contribution value of MSC-Cu-DTHAB.

Conclusions

A novel coordination polymer framework film based on CuO_4 linkage is successfully prepared through the liquid-liquid interface polymerization method. The sample is employed to fabricate flat micro-supercapacitors by laser scribing and exhibits a high volumetric specific capacitance of 121 F cm^{-3} , and the maximum volumetric energy density of 52.6 mWh cm^{-3} . More importantly, the micro-supercapacitors (MSCs) display typical alternating current (AC) line filtering performance (-84.2° at

120 Hz) and a short resistance capacitance (RC) constant (τ_{RC}) of 0.08 ms. This work offers new options for coordination polymer framework film-based MSCs and paves the way for integrated on-chip energy storage devices.

Experimental Section

Materials: Cupric acetate (Adamas, 98%+), ethyl acetate (Adamas 99.8%), LiCl (Adamas, 99%+), polyvinyl alcohol (Adamas, CPS: 4.6–5.4), 1-ethyl-3-methylimidazolium tetrafluoroborate (Adamas, 99%), poly (1,1-difluoroethylene) (Fluorochem), sulfuric acid (Adamas, 96%), *N,N*-dimethylformamide (Adamas, 99.8%), 1-ethyl-3-methylimidazolium tetrafluoroborate (Adamas, 99%), and acetone (Adamas, $\geq 99.5\%$) were commercially purchased. In addition, the monomers DM-THA and DTHAB were synthesized according to the literature.

Synthesis of 9-bromo-2,3,6,7-tetramethoxyanthracene (Br-TMOA): In a 500 mL three-necked round bottom flask, 2,3,6,7-tetramethoxyanthracene (TMOA) (4 g, 13.4 mmol) was dissolved in 300 mL CHCl_3 . CuBr_2 (6 g, 26.8 mmol) was added to the solution, and the reaction was stirred overnight at 70°C . Then, the mixture was filtered, and the solution was concentrated under reduced pressure. It was further purified by column chromatography (silica) with ethyl acetate and petroleum ether as eluent; the final product was obtained as a pale-yellow solid (64% yield).^[25] $^1\text{H NMR}$ (500 MHz, CDCl_3): $\delta = 8.05$ (s, 1H), 7.66 (s, 2H), 7.16 (s, 2H), 4.13 (s, 6H), 4.07 ppm (s, 6H). $^{13}\text{C NMR}$ (500 MHz, CDCl_3): $\delta = 150.74$, 149.52, 127.71, 126.43, 124.38, 122.59, 105.10, 105.04, 55.97 ppm. MS (MALDI-TOF): calculated for $\text{C}_{18}\text{H}_{17}\text{BrO}_4$: 376.03, found: 375.970.

Synthesis of 1,4-bis(2,3,6,7-tetramethoxyanthracen-9-yl)benzene (DTMOAB): In a 250 mL three-necked round bottom flask, a mixture of toluene (36 mL) and EtOH (36 mL) was sparged for 1 h under N_2 , then Br-TMOA (1 g, 2.65 mmol), 1,4-phenylenediboronic acid (200 mg, 1.2 mmol) and $\text{Pd}(\text{PPh}_3)_4$ (278 mg, 0.24 mmol, 5 mol%) were added while sparging for another 30 min. A solution of K_2CO_3 (1.5 g, 10.8 mmol) in H_2O (4 mL) was added to the flask, and then the reaction mixture was refluxed overnight. After the reaction was over, the mixture was first cooled to room temperature. The resulting suspension was filtered and the solid washed successively with H_2O and EtOH. It was further purified by column chromatography (silica) with dichloromethane and petroleum ether as eluent; the final product was obtained as a white solid (42% yield).^[26] $^1\text{H NMR}$ (500 MHz, CDCl_3): $\delta = 8.20$ (s, 2H), 7.72 (s, 4H), 7.27 (s, 4H), 7.03 (d, 4H), 4.10 (s, 12H), 3.81 ppm (s, 12H). $^{13}\text{C NMR}$ (500 MHz, CDCl_3): $\delta = 149.26$, 136.55, 133.07, 131.43, 127.51, 125.94, 122.41, 105.13, 103.68, 55.93, 54.89 ppm. MS (MALDI-TOF): calculated for $\text{C}_{42}\text{H}_{38}\text{O}_8$: 670.26, found: 670.228.

Synthesis of 9,9'-(1,4-phenylene)bis(anthracene-2,3,6,7-tetraol) (DTHAB): In a 250 mL three-necked round bottom flask, DTMOAB (120 mg, 0.179 mmol) was suspended in 30 mL anhydrous dichloromethane under N_2 , and BBr_3 (0.73 mL, 7.5 mmol) was carefully added using a syringe. The mixture was stirred for 4 days at room temperature, then injected slowly with 10 mL H_2O after the reaction was over. The precipitate was collected by centrifugation and washed with dichloromethane for three times. The product was dried under vacuum to give DTHAB as a dark green solid (40% yield).^[27] $^1\text{H NMR}$ (500 MHz, $[\text{D}_6]\text{DMSO}$): $\delta = 10.42$ (s, 8H), 7.44 (d, 4H), 7.48 (s, 2H), 7.19 (s, 4H), 7.09 (s, 4H), 6.98 ppm (s, 4H). MS (MALDI-TOF): calculated for $\text{C}_{34}\text{H}_{22}\text{O}_8$: 558.13, found: 558.17.

Synthesis of 9,10-dimethyl-2,3,6,7-tetrahydroxyanthracene (DM-THA): In a 250 mL three-necked round bottom flask, DM-TMOA (1 g, 3.06 mmol) was suspended in 30 mL anhydrous dichlorome-

thane under N_2 , and BBr_3 (6.07 mL, 64.19 mmol) was carefully added using a syringe. The mixture was stirred for 2 days at room temperature, then injected slowly with 10 mL H_2O after the reaction was over. The precipitate was collected by centrifugation and washed with dichloromethane for three times. The product was dried under vacuum to give DM-THA as a green solid (61% yield).^[27] 1H NMR (500 MHz, $[D_6]DMSO$): δ = 9.41 (s, 4H), 7.34 (s, 4H), 2.70 ppm (s, 6H). ^{13}C NMR (500 MHz, $CDCl_3$): δ = 146.36, 125.71, 121.44, 106.04, 14.63 ppm. MS (MALDI-TOF): calculated for $C_{16}H_{14}O_4$: 270.09, found: 270.096.

Synthesis of Cu-THA: In a 250 mL three-necked round bottom flask, DM-THA (120 mg, 0.44 mmol) and $Cu(OAc)_2$ (129 mg, 0.71 mmol) were added into 150 mL anhydrous DMF under N_2 . The solution was stirred for 24 h at room temperature. After the reaction was over, the mixed solution was filtered and washed with DMF, water, and acetone. Then, the powder was vacuum dried at 60 °C as a dark green powder (denoted as Cu-THA).^[28] Yield: 59%.

Synthesis of Cu-DTHAB: The Cu-DTHAB film was based on systematically placing the reagent solution in a 100 mL container. First, DTHAB was dissolved into ethyl acetate solvent by sonication and filtered out insoluble, $Cu(OAc)_2$ was totally dissolved into deionized water correspondingly. After that, copper acetate aqueous solution ($2.5 \times 10^{-3} \text{ mol L}^{-1}$, 20 mL) was added to the container. A solution of DTHAB in ethyl acetate ($1 \times 10^{-3} \text{ mol L}^{-1}$, 20 mL) was carefully by syringe into the surface of copper acetate aqueous solution. A flat interface was formed as a medium to induce the coordination polymerization. The resulted biphasic solution was reposefully laid for 24 h at room temperature.^[29] Then, the organic layer was removed by using a syringe carefully, and the interfacial film was transferred to substrates. It was soaked carefully in ethyl acetate and water, respectively, and washed three times and air dried. Finally, the Cu-DTHAB film was gained.

Fabrication of Cu-DTHAB based MSCs: First, Au was sputtered onto the surface of a glass sheet based on Magnetron Sputtering System JCP350 with a working power of 150 W and a chamber pressure of approximately 0.5 Pa. The Cu-DTHAB film was transferred onto the Au substrate. Then, the Cu-DTHAB/Au film was laser-scribed to prepare interdigitated electrodes. The electrolyte was carefully appended onto the face of interdigitated electrodes and solidified overnight. Finally, the MSC-Cu-DTHAB was gained successfully. In this work, PVA/LiCl, PVA/ H_2SO_4 , and $[EMIM][BF_4]$ were used as electrolytes.

Acknowledgements

T.Y. and Y.W. contributed equally to this work. This work was financially supported by National Key Research and Development Program of China (2017YFE9134000), NSFC (51973114, 21878188, 21720102002, 51811530013), and Science and Technology Commission of Shanghai Municipality (19JC412600), Greece-China joint R&D project Calypso (T7ΔKI-00039), co-financed by Greece, the EU Regional Development Fund. C.K. thanks the financial support from the Key Science and Technology Project in Henan Province (Innovation Leading Project: 191110210200). D.T. thanks the support from China Postdoctoral Science Fund (2020M671117). J.Z. thanks the support from NSFC (11705270, 11975100). We thank the beamline BL14W1 and BL15U1 of the Shanghai Synchrotron Radiation Facility (SSRF, China) for providing the beamtime.

Conflict of interest

The authors declare no conflict of interest.

Keywords: alternating current line filtering • catechol • coordination polymer framework • copper • micro-supercapacitor

- [1] a) P. Huang, C. Lethien, S. Pinaud, K. Brousse, R. Laloo, V. Turq, M. Respaud, A. Demortière, B. Daffos, P. L. Taberna, B. Chaudret, Y. Gogotsi, P. Simon, *Science* **2016**, *351*, 691–695; b) M. F. El-Kady, V. Strong, S. Dubin, R. B. Kaner, *Science* **2012**, *335*, 1326–1330; c) Z. L. Wang, *Adv. Mater.* **2012**, *24*, 280–285; d) Z. Niu, L. Zhang, L. Liu, B. Zhu, H. Dong, X. Chen, *Adv. Mater.* **2013**, *25*, 4035–4042.
- [2] Y. Yue, N. Liu, Y. Ma, S. Wang, W. Liu, C. Luo, H. Zhang, F. Cheng, J. Rao, X. Hu, J. Su, Y. Gao, *ACS Nano* **2018**, *12*, 4224–4232.
- [3] P. Simon, Y. Gogotsi, *Nat. Mater.* **2020**, *19*, 1151–1163.
- [4] a) J. Chmiola, C. Largeot, P.-L. Taberna, P. Simon, Y. Gogotsi, *Science* **2010**, *328*, 480–483; b) J. Zhao, S. Xu, K. Tschulik, R. G. Compton, M. Wei, D. O'Hare, D. G. Evans, X. Duan, *Adv. Funct. Mater.* **2015**, *25*, 2745–2753.
- [5] a) D. Qi, Y. Liu, Z. Liu, L. Zhang, X. Chen, *Adv. Mater.* **2017**, *29*, 1602802; b) N. A. Kyeremateng, T. Brousse, D. Pech, *Nat. Nanotechnol.* **2017**, *12*, 7–15.
- [6] Z. S. Wu, K. Parvez, X. Feng, K. Müllen, *Nat. Commun.* **2013**, *4*, 2487.
- [7] a) Z.-S. Wu, K. Parvez, S. Li, S. Yang, Z. Liu, S. Liu, X. Feng, K. Müllen, *Adv. Mater.* **2015**, *27*, 4054–4061; b) R. Z. Li, R. Peng, K. D. Kihm, S. Bai, D. Bridges, U. Tumuluri, Z. Wu, T. Zhang, G. Compagnini, Z. Feng, A. Hu, *Energy Environ. Sci.* **2016**, *9*, 1458–1467.
- [8] a) C. Yang, K. S. Schellhammer, F. Ortmann, S. Sun, R. Dong, M. Karakus, Z. Mics, M. Löffler, F. Zhang, X. Zhuang, E. Cánovas, G. Cuniberti, M. Bonn, X. Feng, *Angew. Chem. Int. Ed.* **2017**, *56*, 3920–3924; *Angew. Chem.* **2017**, *129*, 3978–3982; b) K. Jiang, I. A. Baburin, P. Han, C. Yang, X. Fu, Y. Yao, J. Li, E. Cánovas, G. Seifert, J. Chen, M. Bonn, X. Feng, X. Zhuang, *Adv. Funct. Mater.* **2020**, *30*, 1908243.
- [9] a) L. Peng, X. Peng, B. Liu, C. Wu, Y. Xie, G. Yu, *Nano Lett.* **2013**, *13*, 2151–2157; b) J. R. Miller, R. A. Outlaw, B. C. Holloway, *Science* **2010**, *329*, 1637; c) D. Zhao, K. Jiang, J. Li, X. Zhu, C. Ke, S. Han, E. Kymakis, X. Zhuang, *BMC Mater.* **2020**, *2*, 3.
- [10] H. Zhong, K. H. Ly, M. Wang, Y. Krupskaya, X. Han, J. Zhang, J. Zhang, V. Kataev, B. Buchner, I. M. Weidinger, S. Kaskel, P. Liu, M. Chen, R. Dong, X. Feng, *Angew. Chem. Int. Ed.* **2019**, *58*, 10677–10682; *Angew. Chem.* **2019**, *131*, 10787–10792.
- [11] S. Gu, Z. Bai, S. Majumder, B. Huang, G. Chen, *J. Power Sources* **2019**, *429*, 22–29.
- [12] T. He, S. Chen, B. Ni, Y. Gong, Z. Wu, L. Song, L. Gu, W. Hu, X. Wang, *Angew. Chem. Int. Ed.* **2018**, *57*, 3493–3498; *Angew. Chem.* **2018**, *130*, 3551–3556.
- [13] C. Yang, R. Dong, M. Wang, P. S. Petkov, Z. Zhang, M. Wang, P. Han, M. Ballabio, S. A. Brauning, Z. Liao, J. Zhang, F. Schwoitzer, E. Zschech, H. H. Klaus, E. Cánovas, S. Kaskel, M. Bonn, S. Zhou, T. Heine, X. Feng, *Nat. Commun.* **2019**, *10*, 3260.
- [14] Y.-F. Wang, S.-Y. Yang, Y. Yue, S.-W. Bian, *J. Alloys Compd.* **2020**, *835*, 155238.
- [15] S. Bi, Z.-A. Lan, S. Paasch, W. Zhang, Y. He, C. Zhang, F. Liu, D. Wu, X. Zhuang, E. Brunner, X. Wang, F. Zhang, *Adv. Funct. Mater.* **2017**, *27*, 1703146.
- [16] S. Bi, C. Yang, W. Zhang, J. Xu, L. Liu, D. Wu, X. Wang, Y. Han, Q. Liang, F. Zhang, *Nat. Commun.* **2019**, *10*, 2467.
- [17] R. Dong, Z. Zhang, D. C. Tranca, S. Zhou, M. Wang, P. Adler, Z. Liao, F. Liu, Y. Sun, W. Shi, Z. Zhang, E. Zschech, S. C. B. Mannsfeld, C. Felser, X. Feng, *Nat. Commun.* **2018**, *9*, 2637.
- [18] J. Liu, Y. Zhou, Z. Xie, Y. Li, Y. Liu, J. Sun, Y. Ma, O. Terasaki, L. Chen, *Angew. Chem. Int. Ed.* **2020**, *59*, 1081–1086; *Angew. Chem.* **2020**, *132*, 1097–1102.
- [19] M. F. El-Kady, R. B. Kaner, *Nat. Commun.* **2013**, *4*, 1475.
- [20] M. Zhang, Q. Zhou, J. Chen, X. Yu, L. Huang, Y. Li, C. Li, G. Shi, *Energy Environ. Sci.* **2016**, *9*, 2005–2010.

- [21] J. Lin, C. Zhang, Z. Yan, Y. Zhu, Z. Peng, R. H. Hauge, D. Natelson, J. M. Tour, *Nano Lett.* **2013**, *13*, 72–78.
- [22] D. Pech, M. Brunet, H. Durou, P. Huang, V. Mochalin, Y. Gogotsi, P.-L. Taberna, P. Simon, *Nat. Nanotechnol.* **2010**, *5*, 651–654.
- [23] Q. Zhang, M. D. Levi, Y. Chai, X. Zhang, D. Xiao, Q. Dou, P. Ma, H. Ji, X. Yan, *Small Methods* **2019**, *3*, 1900246.
- [24] S. Ardizzone, G. Fregonara, S. Trasatti, *Electrochim. Acta* **1990**, *35*, 263–267.
- [25] R. K. Hallani, V. Fallah Hamidabadi, A. J. Huckaba, G. Galliani, A. Babaei, M.-G. La-Placa, A. Bahari, I. McCulloch, M. K. Nazeeruddin, M. Sessolo, H. J. Bolink, *J. Mater. Chem. C* **2018**, *6*, 12948–12954.
- [26] C. K. Frederickson, L. N. Zakharov, M. M. Haley, *J. Am. Chem. Soc.* **2016**, *138*, 16827–16838.
- [27] Z. Meng, A. Aykanat, K. A. Mirica, *J. Am. Chem. Soc.* **2019**, *141*, 2046–2053.
- [28] J. Park, A. C. Hinckley, Z. Huang, D. Feng, A. A. Yakovenko, M. Lee, S. Chen, X. Zou, Z. Bao, *J. Am. Chem. Soc.* **2018**, *140*, 14533–14537.
- [29] Y. Liu, Z. Xie, W.-Y. Wong, *J. Inorg. Organomet. Polym.* **2020**, *30*, 254–258.

Manuscript received: January 16, 2021

Accepted manuscript online: February 10, 2021

Version of record online: March 5, 2021